PAPER Nr. : 15

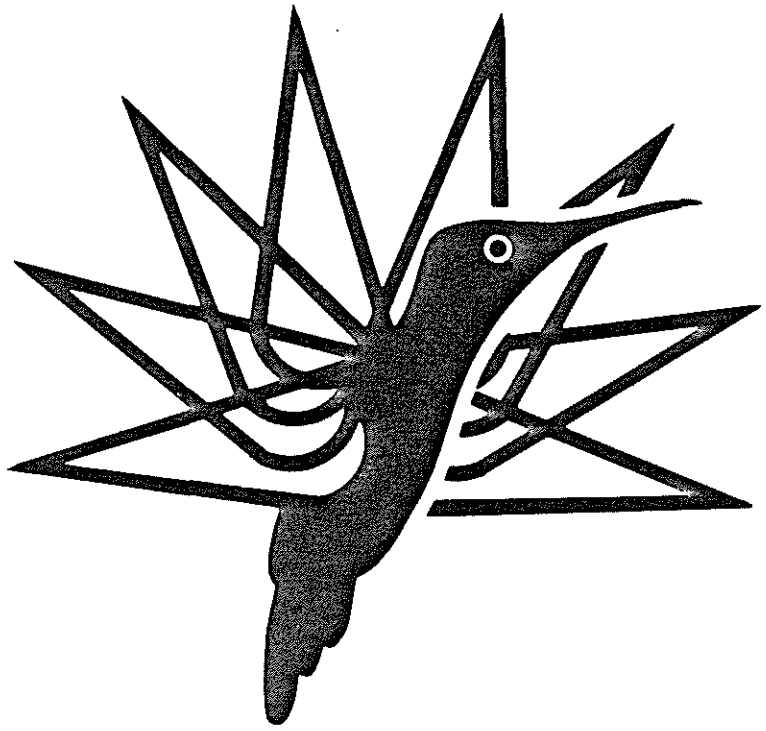

THEORETICAL PREDICTION OF RUNNING-TIME MEASUREMENTS IN UNSTEADY FLOW

BY

W. SEND

German Aerospace Research Establishment (DFVLR)
Institute of Aeroelasticity
Göttingen, W. Germany

TENTH EUROPEAN ROTORCRAFT FORUM

AUGUST 28 – 31, 1984 – THE HAGUE, THE NETHERLANDS

Theoretical Prediction of Running-Time Measurements in Unsteady Flow

by

Wolfgang Send

Abstract

The theoretical prediction of running-time measurements is part of an investigation concerning various blade tip shapes of rotor blades. The results are intended to give a better understanding of vorticity formation and concentration in the wake of a blade. The particular aim of the theoretical research is a closer understanding of vorticity production on a lifting surface and an appropriate description of convected vorticity in unsteady flow. The physical assumptions for the flow are infinitely high Reynolds number and incompressible flow, which lead to a simplified vorticity transport equation. An essential part of the theory is the analytical solution of the three-dimensional wake integral in unsteady flow permitting fast and precise computation of induced velocity fields. The theory describes running-time measurements in front of a profile as well as downstream of it. For various parameters such as reduced frequency, amplitude and steady angle of incidence, theoretical and experimental results are compared for two different profiles.

1. Introduction

The theoretical prediction of running-time measurements is part of an investigation concerning various blade tip shapes of rotor blades. The results are intended to give a better understanding of vorticity formation and concentration in the wake of a blade. The corresponding experiments have been performed in recent years at our research center. The experiments also included unsteady pressure measurements. Some of these results are presented at this forum by my colleague W.J. Wagner [1].

The particular aim of the theoretical research was a closer understanding of vorticity production on a lifting surface and an appropriate description of convected vorticity in unsteady flow. The velocity field induced by the downstream vorticity determines the typical shape of running-time signals. The mathematical model applied to describe the three-dimensional flow around a profile of finite thickness was introduced in a paper presented earlier at this forum [2]. The physical assumptions for the flow are infinitely high Reynolds number and incompressible flow, which lead to a simplified vorticity transport equation. Harmonically varying motion produces harmonically varying vorticity. The interaction between vorticity and the velocity field is traced thoroughly and is illustrated in a 6-minute computer movie.

An essential part of the theory is the analytical solution of the three-dimensional wake integral in unsteady flow permitting fast and precise computation of induced velocity fields. The solution of the integral is now published in full length [3]. The theory describes running-time measurements in front of a profile as well as downstream. For various parameters such as reduced frequency, amplitude and steady angle of incidence, theoretical and experimental results are compared for two different profiles. A comparison shows reasonable agreement between theory and experiment. Fortunately the

most difficult magnitude, the phase lag of the signals, is hit in most cases and gives some confidence in the mathematical model. Moreover independent calculations of total vorticity based on a Hamel-Oseen model for the tip vortex also agree with the predicted calculations within certain limits.

At the present, efforts are being made to extend the still quite restricted geometrical input to a more flexible program. The intended version should be able to allow systematic investigations of various tip shapes and profiles with respect to their influence on the downstream vorticity distribution and induced drag.

2. Theoretical model

The basic idea of the theoretical model is to describe the flow around a body by the vorticity field resulting from an infinitely thin boundary layer. The concept leads to a simplified vorticity transport equation [2,3]. Ampère's theorem, e.g. in [4], relates the well-known doublet potential to the vorticity sheet. The relation is frequently used to compute pressure distributions. However, V. Carstens [5] has proved that unsteady pressures may be calculated without the use of any scalar potential. To demonstrate the relation between vorticity and doublet sheet for the reader more familiar with the doublet potential method, Figure 2 shows the doublet distribution for a plunging plate. The aspect ratio is 5 and the reduced frequency $\omega^* = 0.5$, based on half chord length. The induced potential experiences a jump of precisely the local doublet strength along a line crossing the wake domain or the plate surface.

In Figure 1 the first case (a) shows the domain of viewpoint coordinates, on which the x-component of the induced velocity field v_x is computed. In Figure 3 the real and imaginary parts of v_x are given for this case. The jump in v_x is equal to the local vorticity field perpendicular to the x-direction, i.e. in spanwise direction. In a domain such as case (b) in Fig.1 neither the induced potential nor the induced velocity field contains any discontinuities. The functions show the time-behaviour of waves travelling downstream.

Separate calculations for steady and unsteady flow contribute their share to the complete solution by the principle of superposition. It is fairly obvious that increasing amplitudes and steady angles of incidence magnify the differences between theoretical and experimental results. The theoretical model is linear with respect to both the angle of incidence and the amplitude of the unsteady motion, which in addition is assumed to vary harmonically in time.

3. Formation and convection of vorticity

Incompressible flow may be described completely by the vorticity transport equation. The boundary conditions require vanishing relative velocity on the surface of any moving body. The resulting boundary layer profile of the velocity field expresses the presence of vorticity. In an aerodynamic environment the domain of non-zero vorticity is confined to a very thin envelope covering the whole body, provided that the geometrical shape of the body is streamlined and the curvature of the flow field does not exceed a moderate magnitude. Vorticity, once it has been created, adheres to the particle carrying it, except that diffusion takes place. The particles loaded with vorticity are washed down and form what is called the wake. Several basic as-

sumptions are adopted now to simplify the extremely complicated requirements of the vorticity transport equation which, in fact, is a nonlinear integro-differential equation.

The first assumption concerns the thickness of the domain of non-zero vorticity. The domain is mathematically treated as if it were infinitely thin. The spatially distributed vorticity is flattened to a sheet of vorticity. The simplification is justified by the ratio of two velocities forming the Reynolds number: the velocity of diffusion, i.e. the time in which vorticity is spread out significantly, and the velocity of convection, i.e. the time in which vorticity is carried significantly downstream. The assumption of an infinitely high Reynolds number simply means that there is no time for vorticity to diffuse in the vicinity of the body considered. Diffusion takes place far downstream. The approximation of an infinitely thin wake acting on the moving body may be interpreted as the far-field solution of a thickened wake. The fact that the diffusion term in the vorticity transport equation is omitted does not imply that vorticity plays no role.

Considering the first assumption discussed above the vorticity transport equation still reads:

$$\frac{\partial}{\partial t}\vec{j}(\vec{r},t) + \vec{v}(\vec{r},t) \cdot \operatorname{grad} \vec{j}(\vec{r},t) = \vec{j}(\vec{r},t) \cdot \operatorname{grad} \vec{v}(\vec{r},t) \qquad (1)$$

with

$$\vec{v}(\vec{r},t) = \operatorname{curl} \vec{A}(\vec{r},t)$$

$$\vec{A}(\vec{r},t) = \frac{1}{4\pi} \int_{\text{Vol.}} \frac{\vec{j}(\vec{r}',t)}{|\vec{r} - \vec{r}'|} \cdot dv' \; .$$

In terms of the doublet potential method it is argued that $\operatorname{div} \vec{v} = 0$ in incompressible flow will be fulfilled by $v = \pm \operatorname{grad} \Phi$. The equation $\Delta\Phi = 0$ together with the well-known Kutta condition is finally solved assuming a flat and undistorted wake. In fact this is a remarkably good approximation in many cases of thin profiles and small angles of incidence, as can be seen later on. Commonly ignored are the severe limitations this approximation imposes on the vorticity transport equation which has not changed its nonlinear properties by merely omitting the diffusion term.

If the procedure just mentioned is translated to the vorticity transport equation, it finally reads

$$\frac{\partial}{\partial t}\vec{j}(\vec{r},t) + u_\infty \frac{\partial}{\partial x}\vec{j}(\vec{r},t) = 0 \; , \qquad (2)$$

where u_∞ is the velocity of onset flow. Its application rests on several further assumptions. The following basic phenomena are excluded from the theoretical description if equation (2) is adopted:

- change of the prescribed line of detachment (i.e. the trailing edge),
- occurrence of additional separation lines (e.g. at the wing tip),
- distortion of the wake by its influence on itself (roll-up of the vortex sheet),

- nonlinear effects by large angles of incidence or large amplitudes in unsteady motion.

The well-established "Kutta condition" is replaced by the condition of continuity for the vorticity vector along any line of detachment. Figure 4 shows L. Prandtl's idea of a two-dimensional unsteady wake [6] and the three-dimensional complement used in this paper [3]. Some confidence in the shape of the vorticity field is given by an experimental study of S. Taneda on the structure of the vortex street behind a circular cylinder of finite length [7]. He describes very carefully the way he found the directions of the velocity field (Figure 5). Though in his case the wake is triggered by the instability on the cylinder surface and not by a forced unsteady motion, the principal appearance of the wake phenomena is quite similar. Placing the thumb of the right hand on the vortex lines in Figure 4b, the bent fingers point in the direction of the flow field. Figure 6 and Figure 7 show the real and imaginary parts of j_x and j_y for the example of the plate already introduced. The solution is obtained by dividing the plate surface into 30 x 5 panels and solving the corresponding integral equation of the first kind. A similar procedure leads to the solution for thick profiles. The graphic presentation of the spatially distributed vorticity field on a thick profile causes some difficulties and does not give much more insight into the creation of vorticity. Therefore the plate solution is preferably used to illustrate the mathematical properties. Overall information about the concentration of vorticity is given by a plot of vorticity density on the plate surface and downstream of it. In Figure 8 two shots have been taken from the time-dependent process of vorticity creation and transport. The 0-degree position is the maximum deflection of the plate surface; at 90 degrees the plate passes its position of rest. The maximum vertical speed at this time leads to a strong vortex. There is a slight phase shift depending on reduced frequency and chordwise position. In the computer movie the complete sequence for one cycle can be seen.

4. Description of the experiments

4.1 The running-time measurement

The investigation of flow patterns by means of ultrasonic pulses in steady flow has been developed by D.W. Schmidt [8] and R.H. Engler [9]. The method was extended to include measurements in unsteady flow for the first time in 1980 [11]. The technical background and some initial applications were recently published [10].

The physical principle of the measurement is shown in Figure 9. An ultrasonic pulse is transmitted a fixed distance through a flow field. The given spatial distance of D = 0.5 m between transmitter and receiver produces a time shift of about 0.0015 s under normal atmospheric conditions. A slight variation of these conditions is not as important as the variation of the local velocity by the flow field itself. The pulse is retarded or accelerated due to the velocity field variation tangential to the direction of travel. The expected order of magnitude of the running-time difference Δt can be estimated easily by a simple calculation.

The signal is propagated with the velocity v_p

$$v_p(s) = c_S + v_{rel}(s) \quad , \tag{3}$$

where c_S is the constant speed of sound. The velocity relative and tangential to the signal path is given by

$$v_{rel}(s) = \vec{v}_{rel}(\vec{x}(s),t_0) \cdot \frac{\vec{r}_R - \vec{r}_E}{|\vec{r}_R - \vec{r}_E|} \tag{4}$$

with

$$0 \leq s \leq D , \qquad \vec{r}_E = \vec{r}(0) , \qquad \vec{r}_R = \vec{r}(D) .$$

The arc length s parameterises the signal path from the emitter point s = 0 to the receiver point s = D. The flow pattern is assumed to be "frozen" at the time t_0 during the short period when the signal passes the fluid.

The assumption is justified as long as changes in the flow are small during the time $t_S = D/c_S$. The frequency f of the harmonic motions does not exceed 12 Hz, so that the period for one cycle is large compared to t_S ($t_S \cdot f \lesssim 0.02$). From $ds/dt = v_p(s)$ follows the total running-time t_D for the pulse

$$t_D = \int_0^D \frac{ds}{v_p(s) + c_S} . \tag{5}$$

The running-time difference Δt is defined as

$$\Delta t = t_D - t_S . \tag{6}$$

In all cases considered later on the direction of the pulse is nearly perpendicular to the onset flow. An example gives the order of magnitude of Δt:

Let u_∞ = 20 m/s and c_S = 340 m/s. The flow may be inclined by $\alpha = 1°$. Then

$$\Delta t_\alpha = \frac{D}{u_\infty \sin\alpha + c_S} - t_S \cong -1.5\ \mu s . \tag{7}$$

The order of some microseconds for the running-time difference Δt is typical of all experiments discussed here. The comparison of experimental and theoretical results does not require further explanation. The experiment gives for any configuration and any location of the test beam a well-defined value which is compared to the theoretical result for equivalent conditions.

The average accuracy of the experiments is about $\pm 0.1\ \mu s$ [9]. The limited accuracy is not due to the electronic equipment, but is mainly caused by asymmetries in windtunnel flow. These experiments were all carried out in the 3 x 3 m^2 Low-Speed Windtunnel at the DFVLR in Göttingen.

The accuracy of the theoretical results is not primarily defined by the numerical integration of equation (5), which can be assumed to be exact. The physical simplifications discussed in Chapter 3 form the intrinsic and unavoidable inaccuracies.

4.2 The models

The theoretical results refer to two different experiments. The NACA 0010 wing was investigated by Engler [9]. The size of the model is given in Figure 10. The wing was suspended from wires connected to the model at the points P_1, P_2 and P_3.

The second model is a NACA 0012 half model with a chordlength of 0.4 m and a span of 0.8 m. The model was mounted on a splitter plate to achieve nearly two-dimensional flow on one side. Theoretically the model was treated as a freestream model with an aspect ratio of 4. The experimental results are partly yet unpublished. Some of the data are reported in [10,11].

5. Results

5.1 NACA 0010, steady flow

The wind speed u_∞ is 20 m/s. Figure 11 shows the running-time difference six chordlengths downstream of the wing for two angles of incidence -4° and -8°. The region near the tip shows interesting details which are not covered by the present theory. The roll-up of the vortex sheet will affect that domain. Based on a semi-empirical Hamel-Oseen model for the tip vortex, Engler has calculated the strength of the tip vortex [9]. The total circulation of the theoretical model exceeds the experimental data:

α	$\Gamma_{exp.}$ [m²/s] (Tip)	$\Gamma_{theor.}$ [m²/s] (Total)
-4°	-0.42	-0.55
-8°	-0.84	-1.10

(8)

It should be pointed out that the basis of the calculations is very different for the two models. The tip vortex will not contain all of the washed down vorticity. But the the theoretical model gives merely an ambiguous answer to the question, which part of the vortex sheet belongs to the region of the tip vortex. The lift coefficients for the 4° case (based on α and chordlength c) are

$$\text{exp.} : \quad c_a = \frac{\Gamma_{exp.}}{c \cdot \alpha \cdot u_\infty/2} = 3.85$$

$$\text{theor.} : \quad c_a \text{ (computed)} = 3.49 \,. \tag{9}$$

The values differ by about 9%. The computed solution follows the method described in [2]. There are 30 panels in circumferential direction times 7 panels in spanwise direction.

In Figure 12 Δt is plotted ahead of the leading edge. The 8° case shows a small systematic difference of about 0.2 µs. However, the slope of the decrease in Δt is represented very well. The 4° case seems to have an error of a factor of 2 in the experimental data. The original values (o) are plotted as well as the corrected ones (c).

5.2 NACA 0012, steady flow

Figure 13 is similar to Fig.11. The angle of incidence is 5° and the downstream position is changed from x/c = 0.5 to x/c = 3. Unfortunately measurements have been taken only in the tip region. The case x/c = 0.5 again shows a systematic difference of about 1.5 μs. The reason might be a normalisation error. It is also possible that the description of the tip region is incomplete quite close to the trailing edge. The case x/c = 3 also tends to deviate slightly from the theoretical curve. However, the overall behaviour of the functions agrees quite well with the experimental results and proves that the theoretical model is a reasonable description of some basic properties of the flow.

5.3 NACA 0012, unsteady flow

The most interesting aspect of the measurements in unsteady flow is - from a theoretical point of view - the variation of phase shift. Data are given for two different frequencies 4 Hz and 12 Hz. In the 12 Hz case ($\omega^* = 0.75$) the downstream positions x/c = 0.5 and x/c = 3.0 are compared again. In Figure 14 and Figure 15 the variation of Δt during one cycle of a pitching motion at two fixed positions is plotted. The two spanwise positions are half a chordlength inside and outside the wake. The tip vortex is located at y = 0 and the positive y-axis points into the wake. As expected the variation of Δt almost vanishes outside the wake domain for the small amplitude of $\Delta\alpha = 1°$. The steady angle of incidence is 5°. Figure 16 is a combination of the last two graphs for the y-position inside the wake. It shows the true velocity of the wake. To calculate the wake velocity, the maximum of Δt may be considered. At x/c = 0.5 its phase is about 320°. At x/c = 3.0 the phase changed to 180°. The increase is $\Delta\phi = 220°$. One cycle is completed in T = 1/12 s. The spatial distance between the two positions is exactly $\Delta s = 1$ m. Therefore the relative velocity of the wake is

$$v_{rel} = \frac{\Delta s}{T \cdot \Delta\phi / 360°} = 19.6 \text{ m/s} . \qquad (10)$$

The result is very important for the justification of a basic assumption in the theoretical model: the velocity of the wake is assumed to be approximately u_∞. Secondly the result reflects the loss in momentum; the wake is slightly accelerated with respect to an observer at rest.

Lastly, Figure 17 exemplifies the influence of a large amplitude. The 4 Hz case ($\omega^* = 0.25$) has zero angle of incidence and an amplitude of $\Delta\alpha = 8°$. The predicted running-time differences differ considerably from the experimental results obtained. The wake is presumably distorted.

6. Conclusion

A suitable approximation of the vorticity transport equation gives immediate insight into the creation and transport of vorticity on a lifting surface. In incompressible flow vorticity is the basic variable governing the whole flow field. Experimental results can be interpreted very easily in terms of vorticity.

The mathematical model of unsteady flow around three-dimensional wings allows the prediction of running times of ultrasonic pulses. The predicted results agree fairly well with experiments carried out in recent years at the DFVLR in Göttingen. The ultrasonic method is very sensitive to small variations of the flow field. It admits a fast and cost-effective investigation of flow patterns in steady and unsteady flow. The further extension of the theoretical approach to a more flexible geometry should be able to allow systematic research on optimised tip shapes with respect to their influence on the downstream vorticity distribution and induced drag.

7. References

[1] W.J. Wagner, Comparative Measurements of the Unsteady Pressures and the Tip-Vortex Parameters on Four Oscillating Wing-Tip Models, Paper No.9 at this forum, 1984.

[2] W. Send, Higher-Order Panel Method Applied to Vorticity-Transport Equation, Fifth European Rotorcraft and Powered Lift Aircraft Forum, Amsterdam 1979.

[3] W. Send, Der instationäre Nachlauf hinter schlanken Auftriebskörpern in inkompressibler Strömung, ZAMM 64, 1984, S.7-15.

[4] E. Martensen, Potentialtheorie, B.G. Teubner, Stuttgart 1968.

[5] V. Carstens, Die Berechnung der instationären Druckverteilung an einem schwingenden Gitter mit dicken Profilen und stationärer Umlenkung, DFVLR-FB 81-38, 1981.

[6] L. Prandtl, Über die Entstehung von Wirbeln in der idealen Flüssigkeit, mit Anwendung auf die Tragflügeltheorie und andere Aufgaben, in: Th.v.Karman und T.Levi-Civita, Vorträge aus dem Gebiet der Hydro- und Aerodynamik, (Innsbruck 1922), Springer Verlag, Berlin 1924.

[7] S. Taneda, Studies on Wake Vortices (I), Reports of Research Institute for Applied Mechanics, Vol.I, 4, Kyushu University, Fukuoku/Japan 1952, pp.131-144.

[8] D.W. Schmidt, Akustische Messung der Zirkulation von Wirbeln und Zirkulationsverteilungen bei Modelluntersuchungen in Windkanälen, Mitt. MPI für Strömungsforschung und AVA, Nr.61, Göttingen 1975.

[9] R.H. Engler, Untersuchungen von Randwirbeln mittels Ultraschall im Nahbereich hinter einem Rechteckflügel im Windkanal, MPI für Strömungsforschung, Bericht 11/1979, Göttingen 1979.

[10] R.H Engler, D.W. Schmidt, W.J. Wagner, B. Weitemeier, Ultrasonic Method for Flow Field Measurement in Windtunnel Tests, J.Acoust.Soc.Am. 71(1), 1982 pp.42-50.

[11] R.H. Engler, et al., Experimental Study of the Tip Vortices behind an Oscillating Blade by the Ultrasonic Method, Proc. of the colloquium honoring Hans Georg Küssner on the occasion of his 80th birthday, Göttingen 1980.

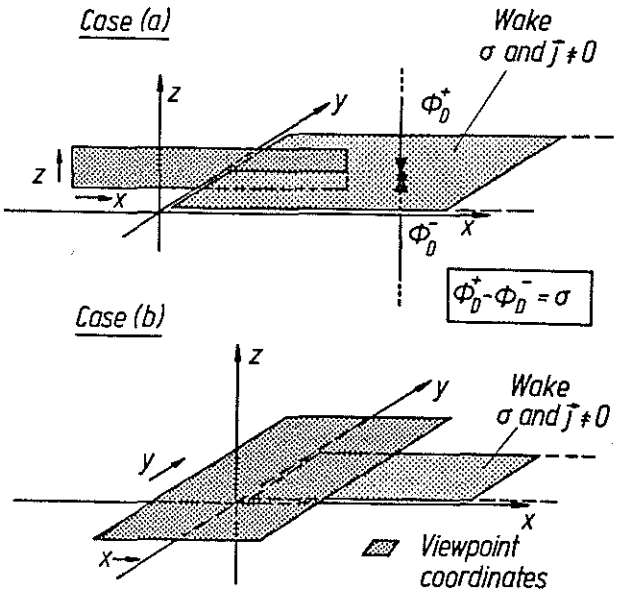

Figure 1: Domain of viewpoint coordinates
a) across the wake
b) above the wake

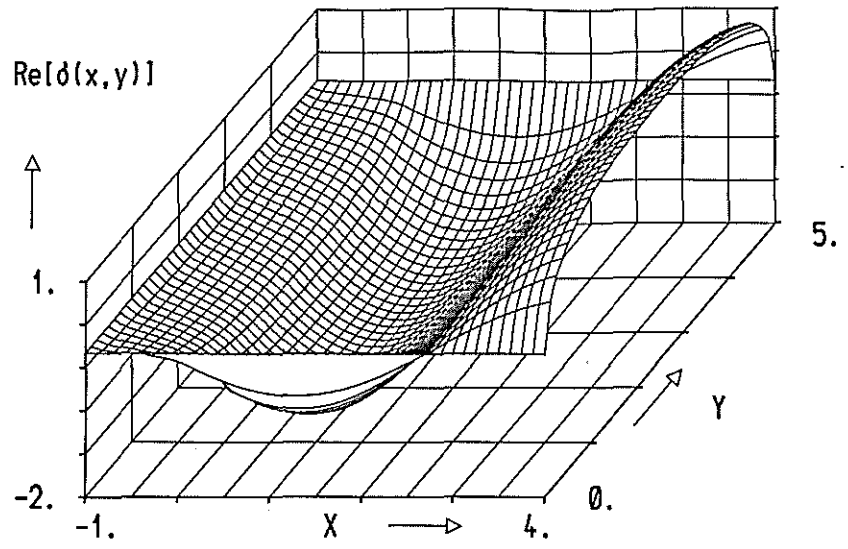

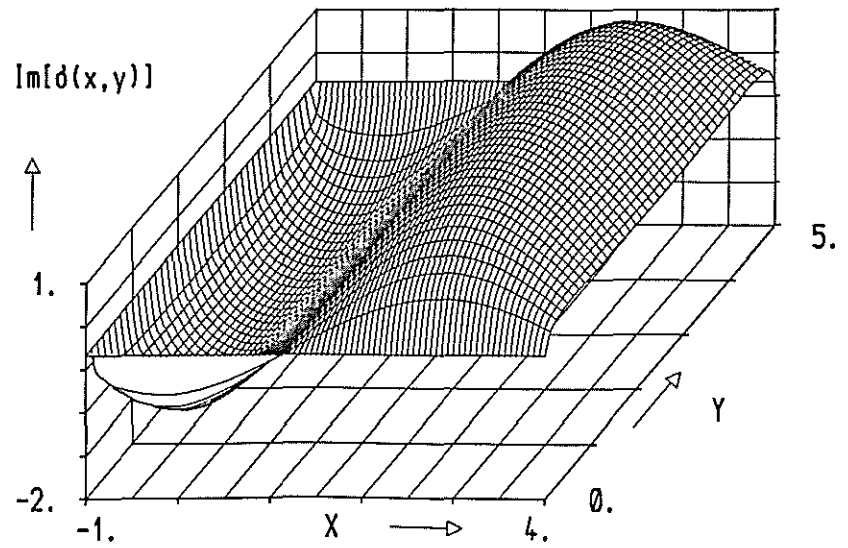

Figure 2: Doublet distribution, $\omega^* = 0.5$, $\ell = 1$, $d = 5$

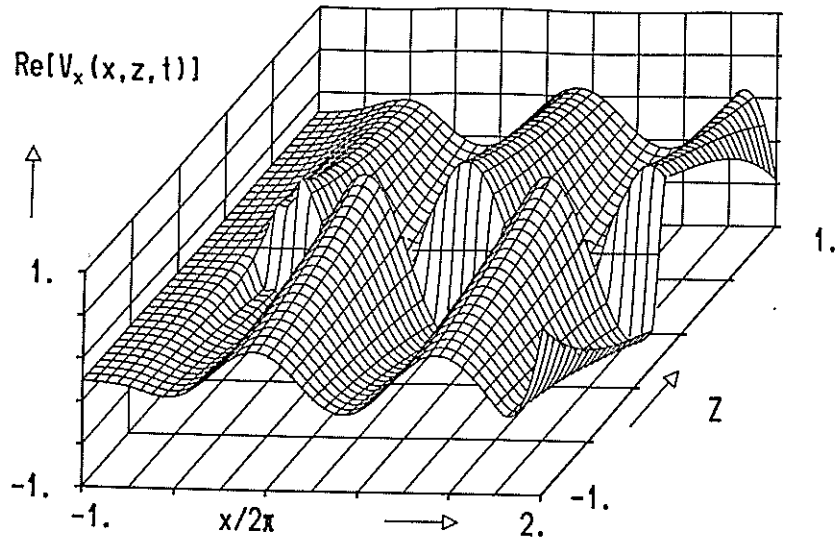

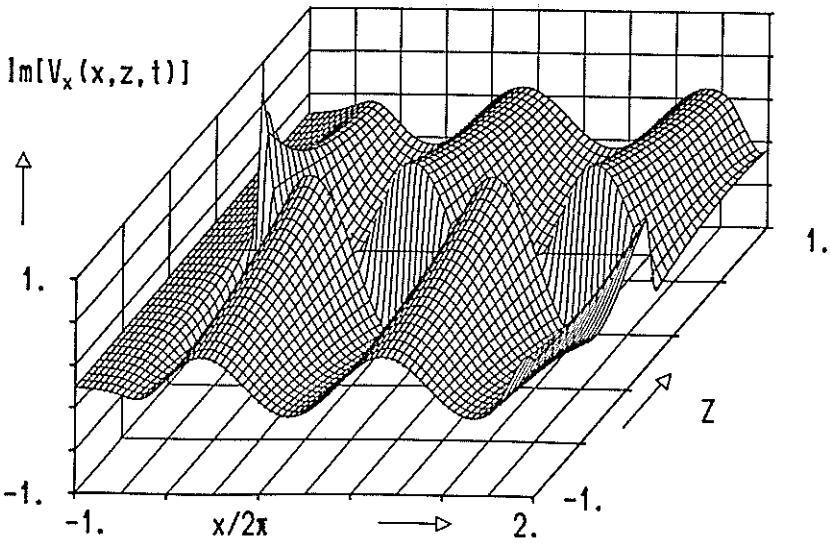

Figure 3: Induced velocity across the wake, $\omega^* = 0.5$, $y = d/2$, $d = 5$

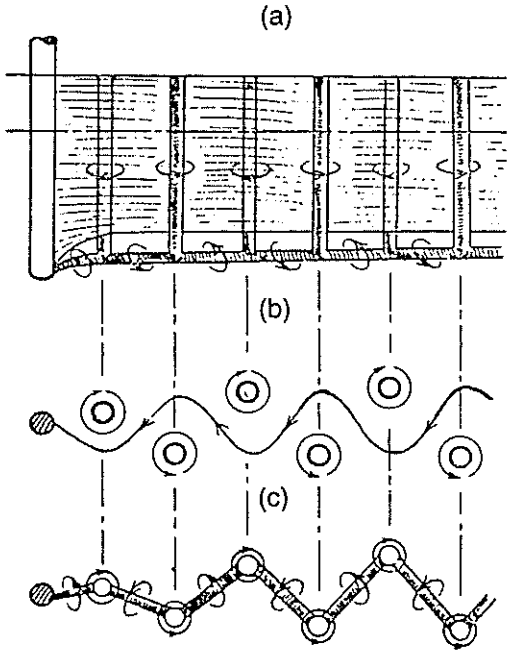

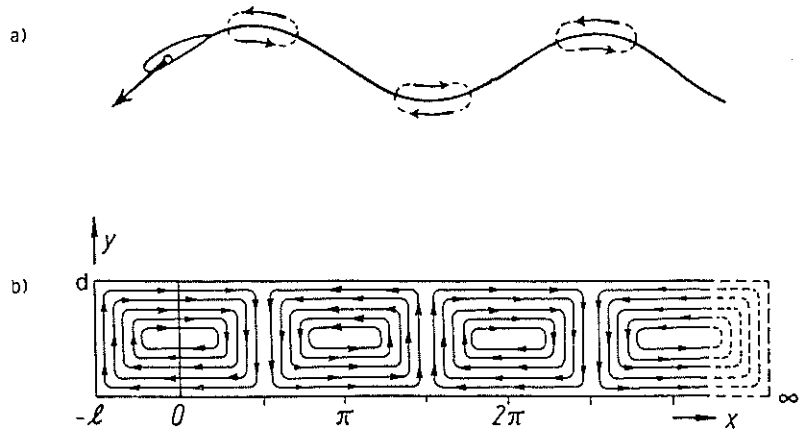

Figure 4: Unsteady wake a) two-dimensional (L.Prandtl)
b) three-dimensional

Figure 5: Structure of the wake behind a circular cylinder (S.Taneda)

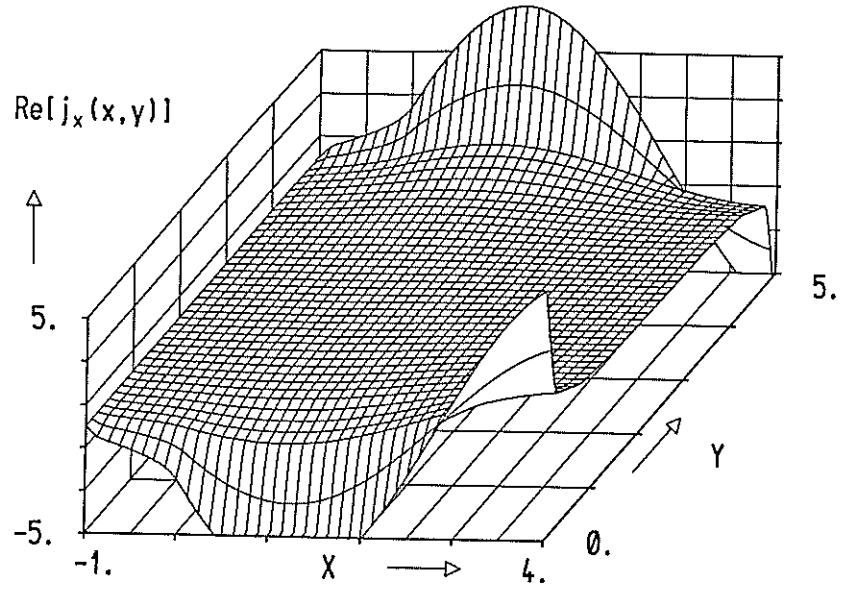

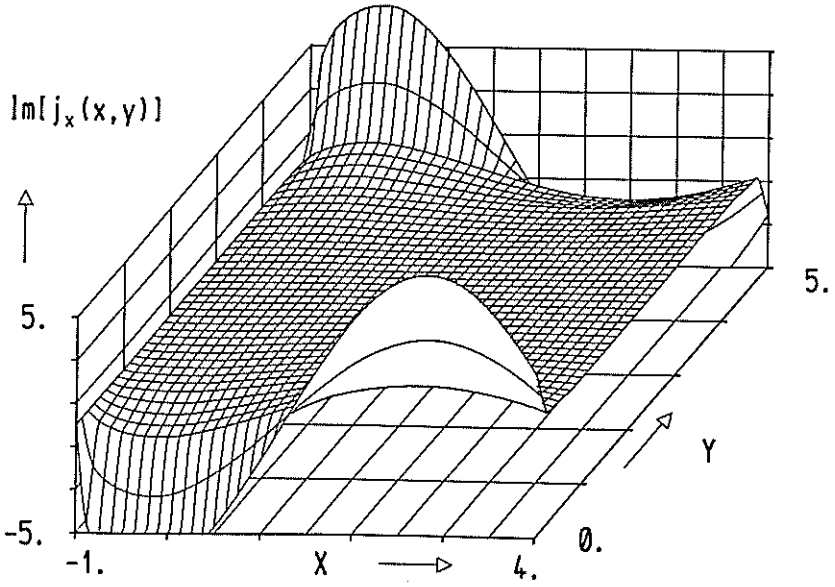

Figure 6: Vorticity vector (plunging plate)
x-component, $\omega^* = 0.5$, d = 5

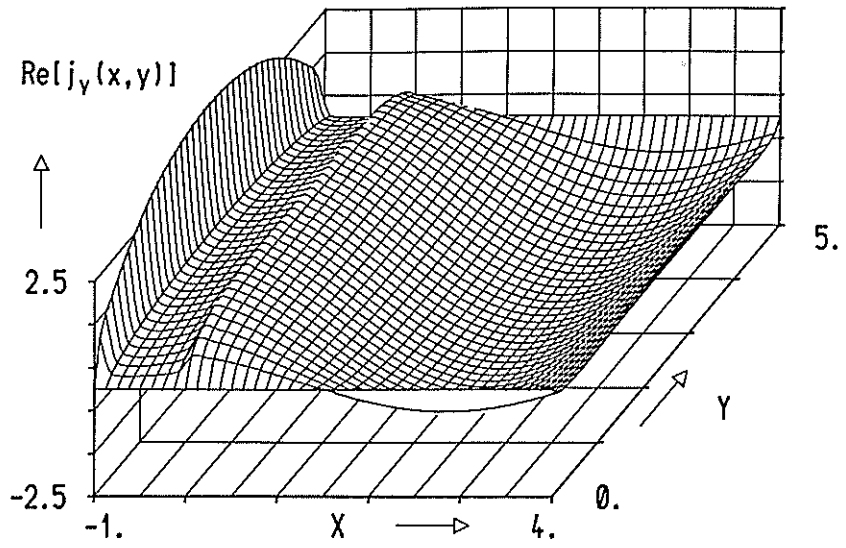

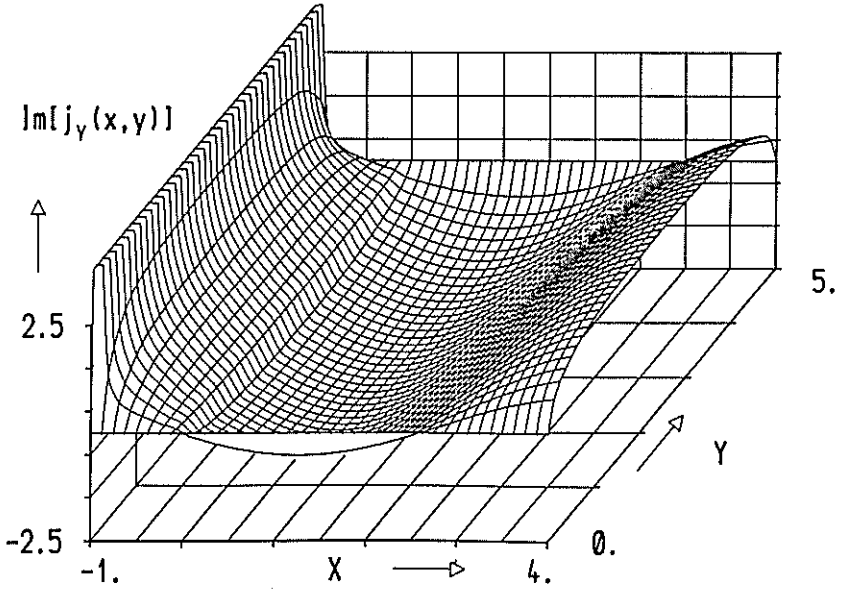

Figure 7: y-component

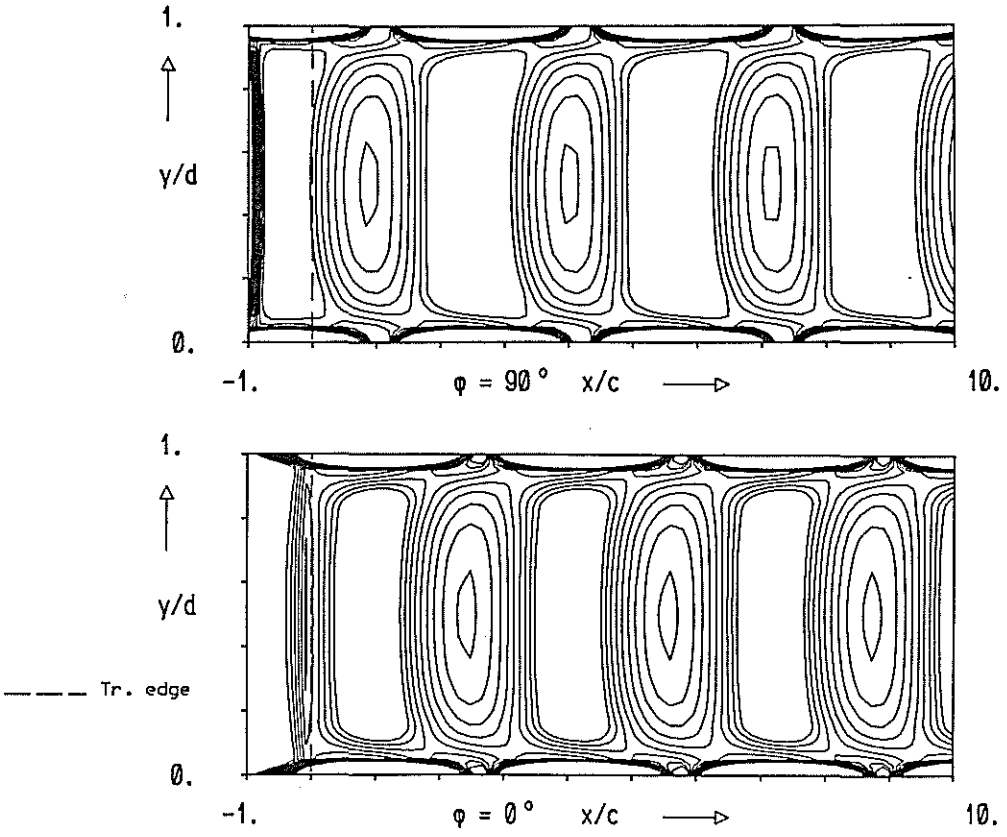

Figure 8: Unsteady vorticity density, $\omega^* = 0.5$, $\ell = 1$, $d = 5$ (plunging plate)

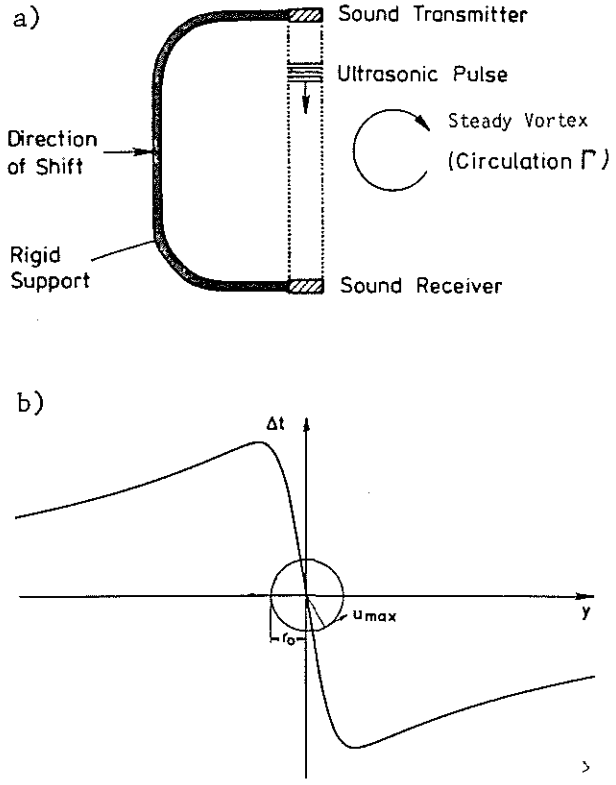

Figure 9: Running-time measurement

a) schematic diagram of the experimental device
b) resulting difference for a steady vortex

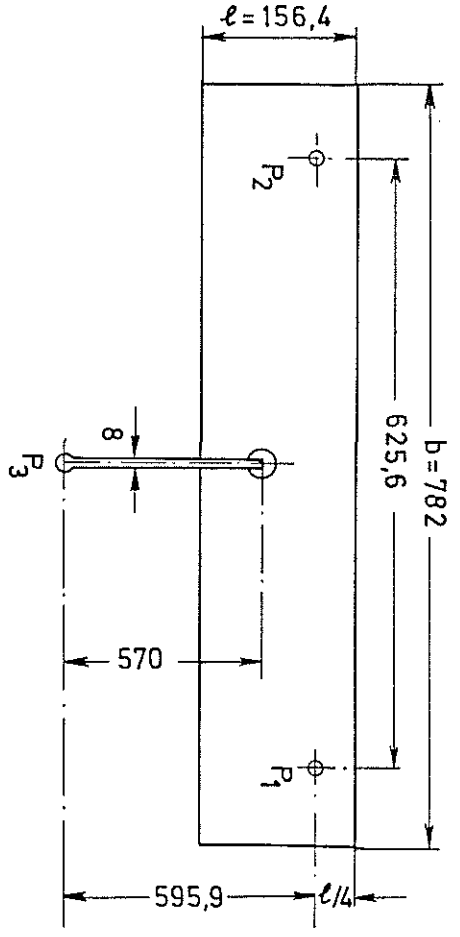

Figure 10: Geometry of the NACA 0010 profile (all dimensions in mm)

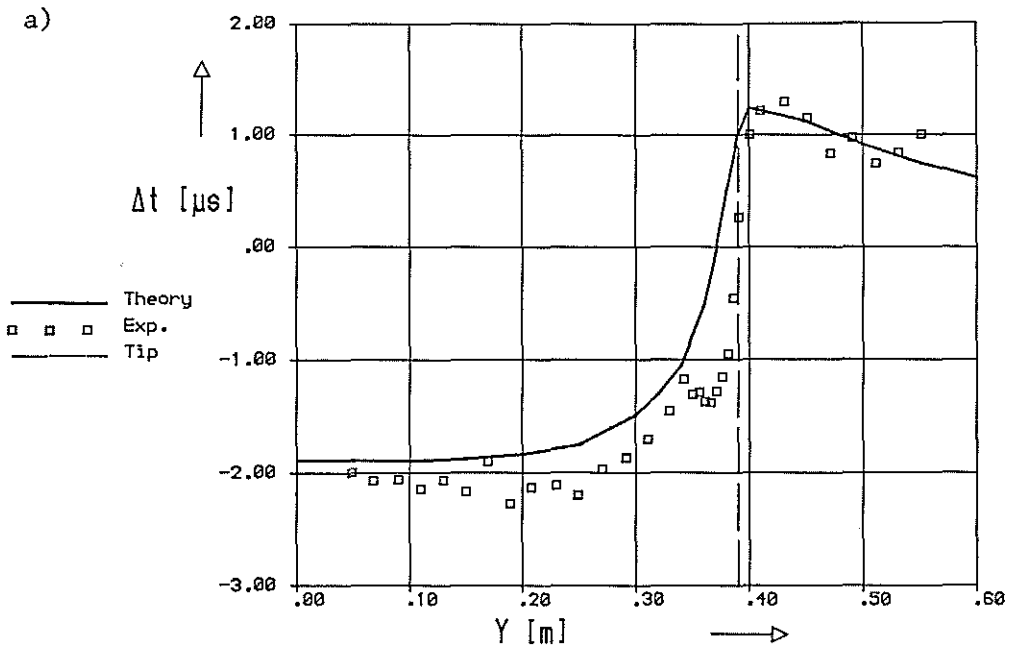

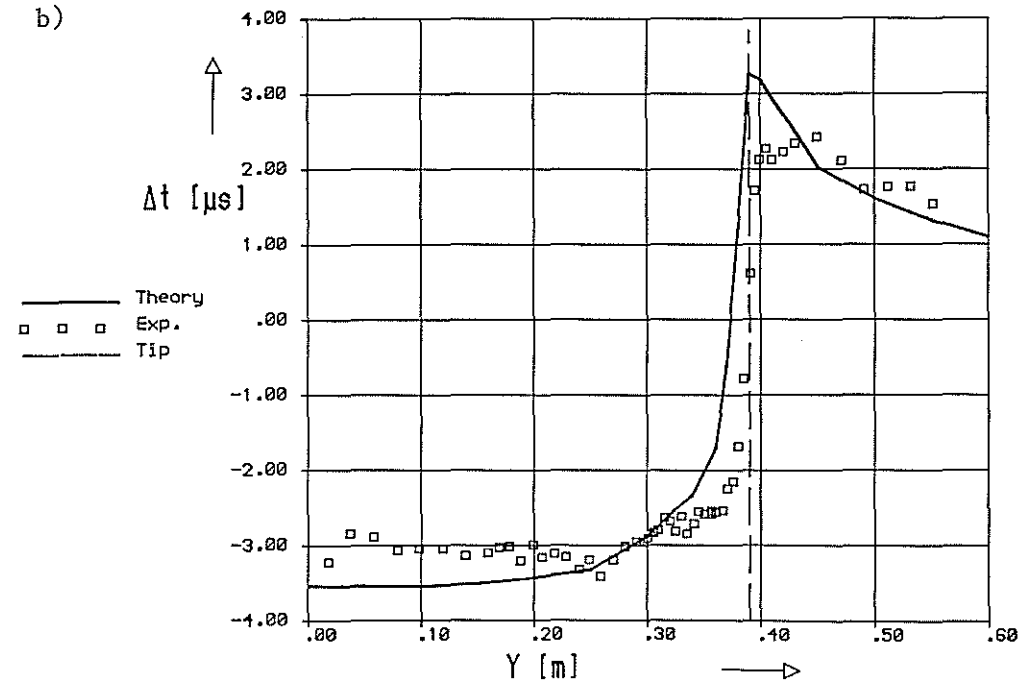

Figure 11: Running time in the wake, NACA 0010, x/c = 6.0

a) $\alpha = -4°$
b) $\alpha = -8°$

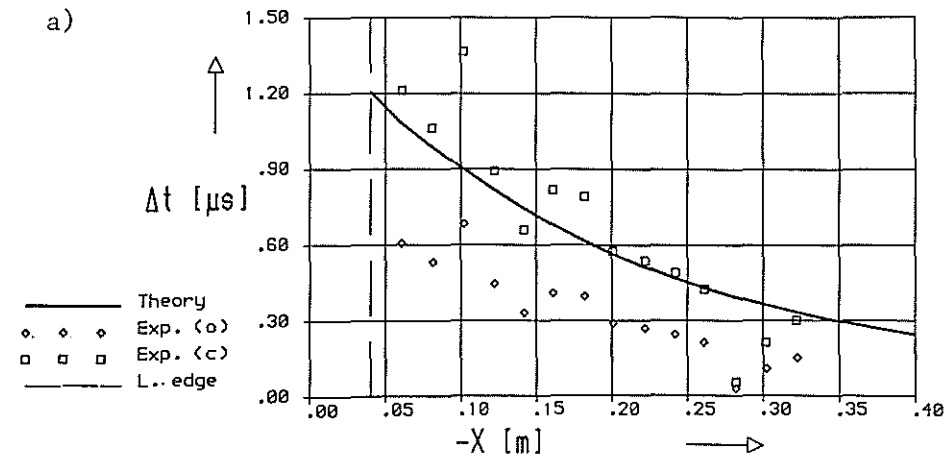

Figure 12: Running time in front of the profile, NACA 0010, y/c = 0.10

a) $\alpha = -4°$

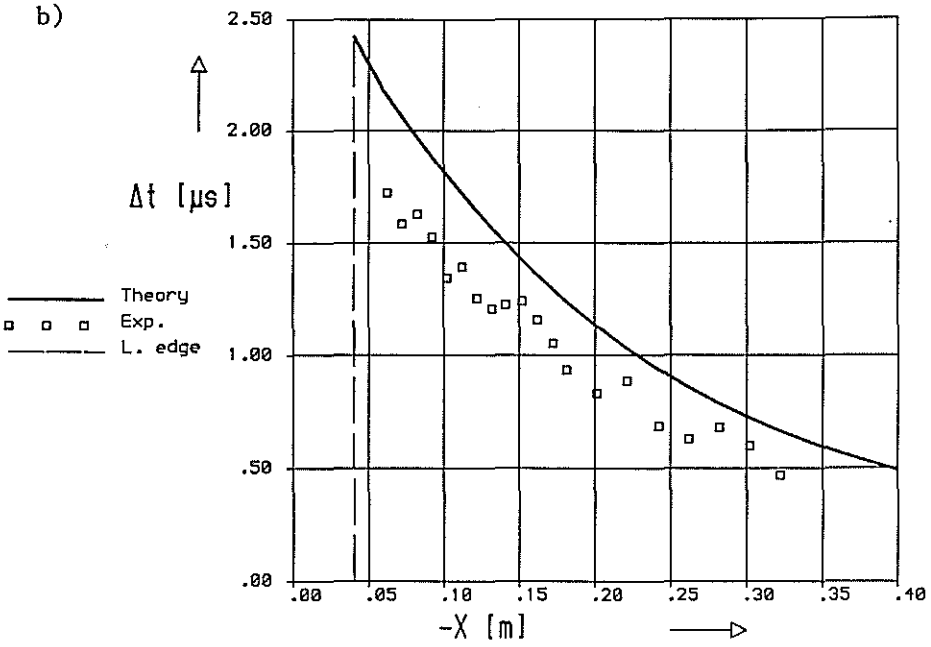

Figure 12 (continued): Running time in front of the profile, NACA 0010, y/c = 0.10

b) $\alpha = -8°$

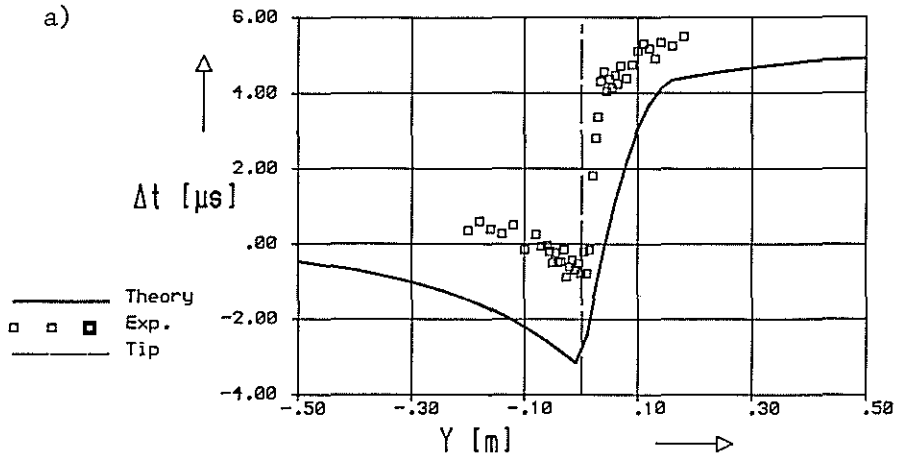

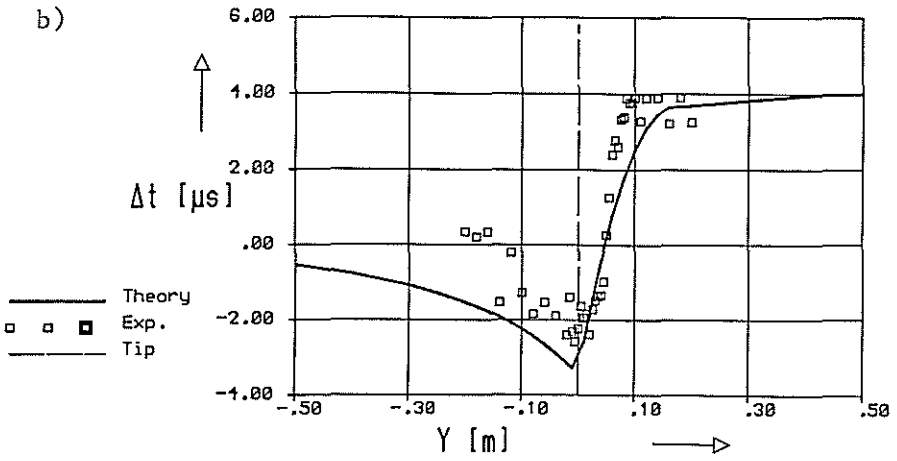

Figure 13: Running time in the wake, NACA 0012

a) x/c = 0.5
b) x/c = 3.0

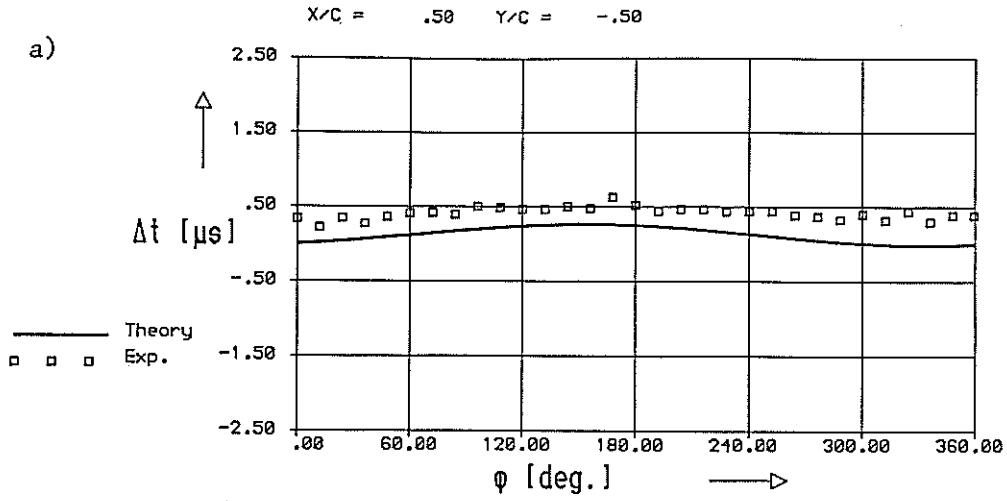

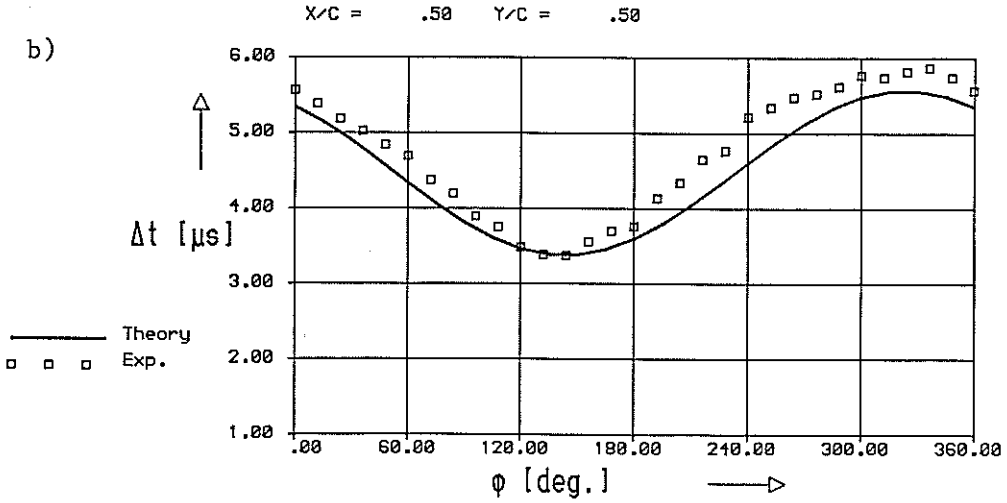

Figure 14: Running time in unsteady flow, NACA 0012, $\alpha = 5°$, $\Delta\alpha = 1°$, $\omega^* = 0.75$, $x/c = 0.5$

a) position outside the wake ($y/c = -0.5$)
b) position inside the wake ($y/c = +0.5$)

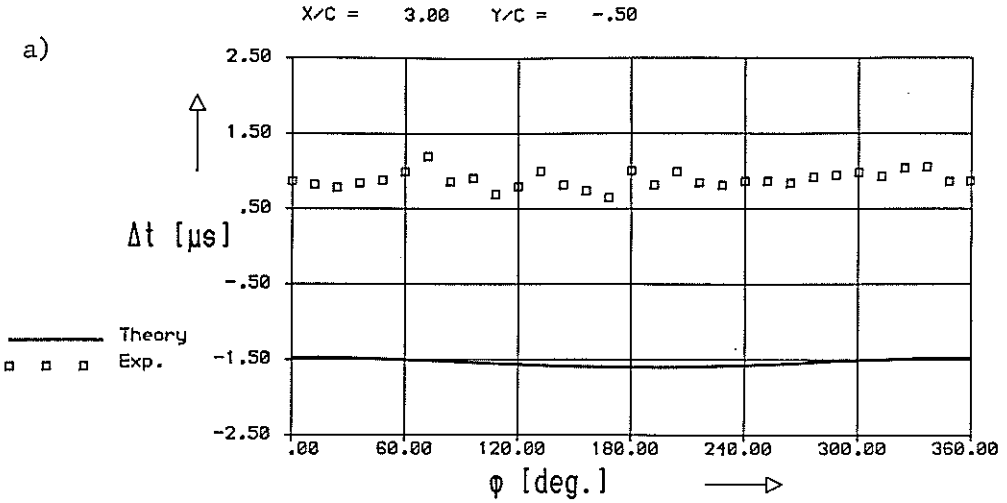

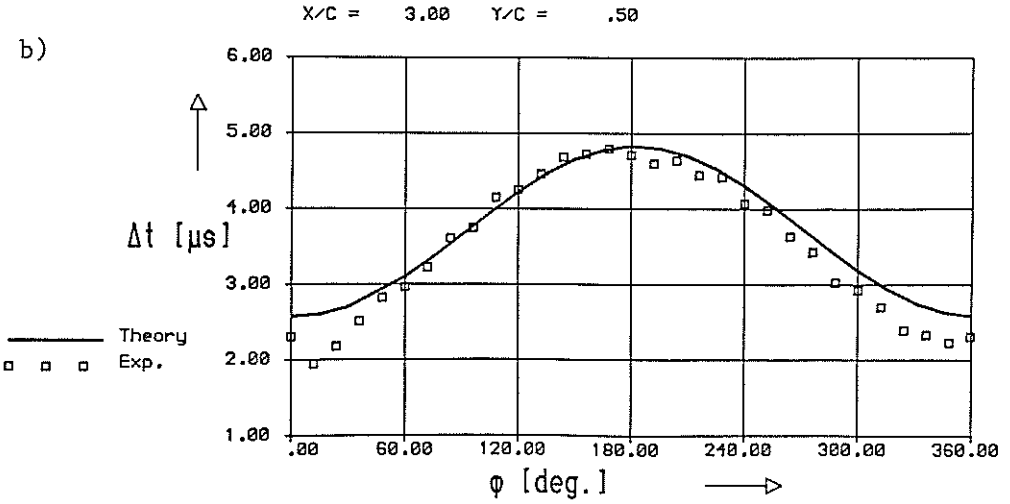

Figure 15: Running time in unsteady flow, NACA 0012, $\alpha = 5°$, $\Delta\alpha = 1°$, $\omega^* = 0.75$, $x/c = 3.0$

a) position outside the wake ($y/c = -0.5$)
b) position inside the wake ($y/c = +0.5$)

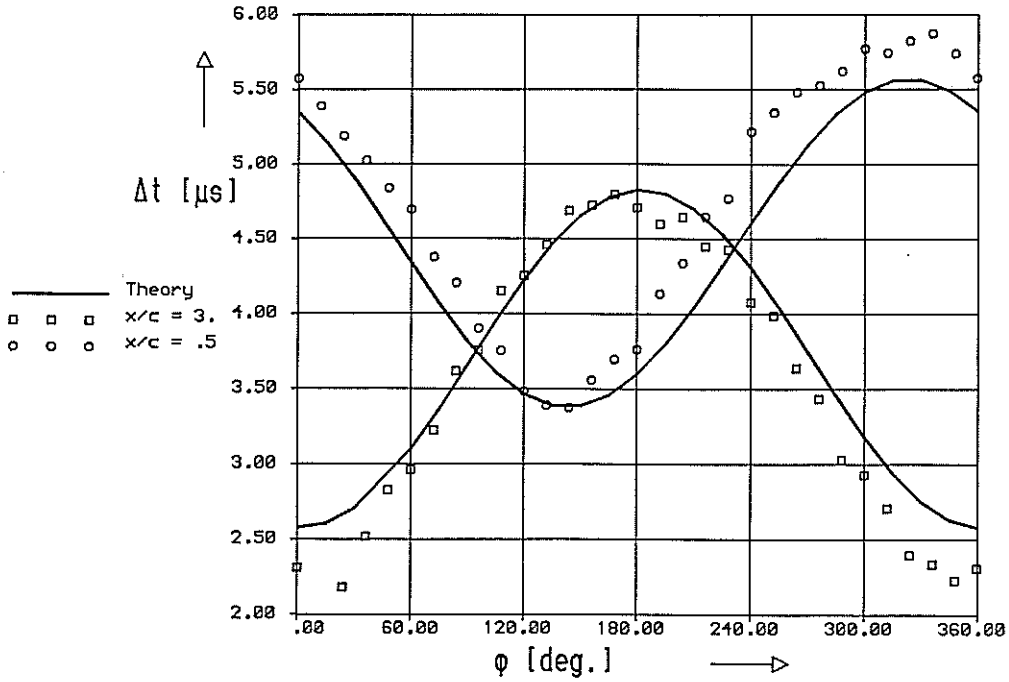

Figure 16: Running time in unsteady flow, NACA 0012, $\alpha = 5°$, $\Delta\alpha = 1°$, $\omega^* = 0.75$, (two different positions downstream of the profile)

a)

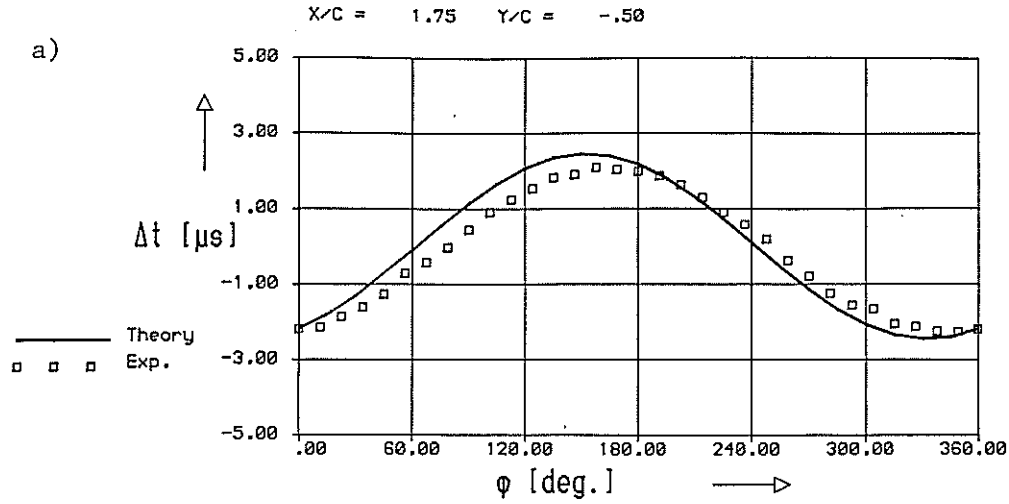

b)

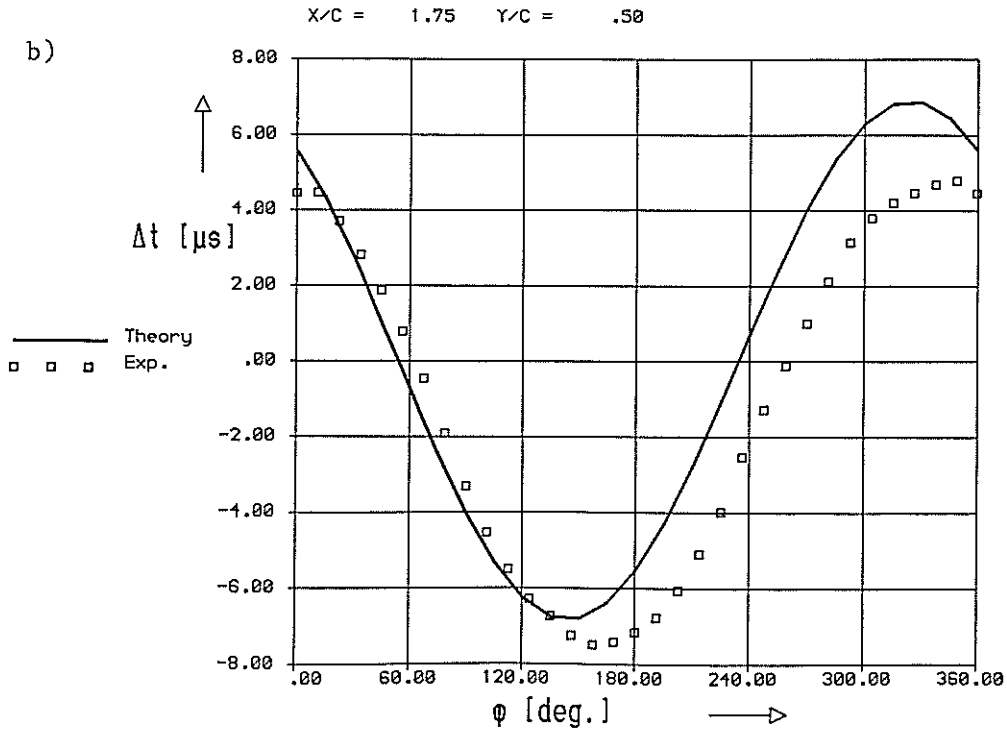

Figure 17: Running time in unsteady flow, NACA 0012, $\alpha = 0°$, $\Delta\alpha = 8°$, $\omega^* = 0.25$, $x/c = 1.75$

a) position outside the wake ($y/c = -0.5$)
b) position inside the wake ($y/c = +0.5$)